Title

Effects of spatial variability in vegetation phenology, climate, landcover, biodiversity, topography, and soil property on soil respiration across a coastal ecosystem.

Journal

Vaccine Reports, 10(9)

ISSN

2405-8440

Authors

He, Yinan

Bond-Lamberty, Ben

Myers-Pigg, Allison

et al.

Publication Date

2024-05-15

DOI

10.1016/j.heliyon.2024.e30470

Peer reviewed

Heliyon 10 (2024) e30470

Contents lists available at ScienceDirect

Heliyon

journal homepage: www.cell.com/heliyon

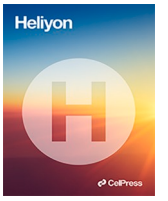

Research article

Effects of spatial variability in vegetation phenology, climate, landcover, biodiversity, topography, and soil property on soil respiration across a coastal ecosystem

Yinan He [a,*], Ben Bond-Lamberty [b], Allison N. Myers-Pigg [c,d], Michelle E. Newcomer [a], Joshua Ladau [e], James R. Holmquist [f], James B. Brown [e], Nicola Falco [a]

[a] Earth and Environmental Sciences Area, Lawrence Berkeley National Laboratory, 1 Cyclotron Road, Berkeley, CA, 94720-8126, USA
[b] Joint Global Change Research Institute, Pacific Northwest National Laboratory, College Park, MD, 20740, USA
[c] Marine and Coastal Research Laboratory, Pacific Northwest National Laboratory, Sequim, WA, 98382, USA
[d] Department of Environmental Sciences, University of Toledo, Toledo, OH, 43606, USA
[e] Computational Biosciences Group, Lawrence Berkeley National Laboratory, 1 Cyclotron Road, Berkeley, CA, 94720, USA
[f] Smithsonian Environmental Research Center, 647 Contees Wharf Road, Edgewater, MD, 21037, USA

ARTICLE INFO

Keywords:
Remote sensing
Harmonized Landsat Sentinel-2
Hierarchical Agglomerative Clustering (HAC)
Post hoc hypothesis test
Random Forest (RF)
SHapley Additive exPlanations (SHAP)

ABSTRACT

Coastal terrestrial-aquatic interfaces (TAIs) are crucial contributors to global biogeochemical cycles and carbon exchange. The soil carbon dioxide (CO_2) efflux in these transition zones is however poorly understood due to the high spatiotemporal dynamics of TAIs, as various sub-ecosystems in this region are compressed and expanded by complex influences of tides, changes in river levels, climate, and land use. We focus on the Chesapeake Bay region to (i) investigate the spatial heterogeneity of the coastal ecosystem and identify spatial zones with similar environmental characteristics based on the spatial data layers, including vegetation phenology, climate, landcover, diversity, topography, soil property, and relative tidal elevation; (ii) understand the primary driving factors affecting soil respiration within sub-ecosystems of the coastal ecosystem. Specifically, we employed hierarchical clustering analysis to identify spatial regions with distinct environmental characteristics, followed by the determination of main driving factors using Random Forest regression and SHapley Additive exPlanations. Maximum and minimum temperature are the main drivers common to all sub-ecosystems, while each region also has additional unique major drivers that differentiate them from one another. Precipitation exerts an influence on vegetated lands, while soil pH value holds importance specifically in forested lands. In croplands characterized by high clay content and low sand content, the significant role is attributed to bulk density. Wetlands demonstrate the importance of both elevation and sand content, with clay content being more relevant in non-inundated wetlands than in inundated wetlands. The topographic wetness index significantly contributes to the mixed vegetation areas, including shrub, grass, pasture, and forest. Additionally, our research reveals that dense vegetation land covers and urban/developed areas exhibit distinct soil property drivers. Overall, our research demonstrates an efficient method of employing various open-source remote sensing and GIS datasets to comprehend the spatial variability and soil respiration mechanisms in coastal TAI. There is no one-size-fits-all approach to modeling carbon fluxes

* Corresponding author
E-mail address: yinan.he@lbl.gov (Y. He).

https://doi.org/10.1016/j.heliyon.2024.e30470
Received 31 October 2023; Received in revised form 21 March 2024; Accepted 26 April 2024
Available online 27 April 2024

released by soil respiration in coastal TAIs, and our study highlights the importance of further research and monitoring practices to improve our understanding of carbon dynamics and promote the sustainable management of coastal TAIs.

1. Introduction

Coastal terrestrial–aquatic interfaces (TAIs) are the transitional zones of land and ocean realms that serve as critical links between coastal terrestrial and aquatic habitats [1]. These interfaces include a range of environments, spanning uplands, wetlands, and coastlines that compress and expand in their spatial extent in response to tides, river-level changes, climate, wetland restoration, and land use [2–6]. Coastal TAIs experience highly dynamic and fluctuating water levels and are characterized by unique hydrological, geomorphological, and ecological processes, influenced by the interactions between land, freshwater, and marine systems [7–11]. Although coastal TAIs occupy relatively small areas of the Earth's surface (approximately 0.07–0.22 %), their impact on local biogeochemical cycles and land-atmosphere carbon exchange is disproportionately significant [12]. Notably, vegetated coastal ecosystems account for a minimum of 50 % of the organic carbon found in marine sediments and export an estimated annual range of 174–400 Tg of organic carbon to the ocean [13,14]. Furthermore, coastal wetland ecosystems emit CO_2 ranging from 150 to 1020 Tg per year [15,16]. Due to their ecological significance, coastal TAIs are also of great importance for carbon conservation and sustainable management efforts, exhibiting characteristics that enhance their carbon sequestration potential.

1. High primary production: Coastal TAIs are highly productive ecosystems and support abundant plant growth and photosynthesis, resulting in the accumulation of organic carbon in their biomass [17,18].
2. Anoxic conditions: Coastal TAIs (such as mangroves and certain wetlands) experience waterlogging or periods of oxygen deprivation (anoxic conditions). In such environments, the decomposition of organic matter is slowed down, reducing the release of carbon dioxide into the atmosphere, and promoting carbon storage [19,20].
3. Sediment trapping: Coastal TAIs act as barriers that trap and retain sediment transported from the land. The organic carbon present in these sediments becomes buried and preserved over time, contributing to long-term carbon sequestration [21,22].

Thus, coastal TAIs are a crucial component of the local ecosystem and contribute significantly to the net carbon balance, playing a vital role in regulating atmospheric CO_2 concentrations.

Soil respiration (Rs) is an essential component of the Earth's ecosystem functioning and a fundamental process in the exchange of CO_2 between land and the atmosphere. It comprises the second most significant flux following gross primary productivity [23,24]. Rs refers to the total efflux of CO_2 from soils into the atmosphere as a result of belowground biological and physicochemical processes [25,26]. Almost all previous Rs research has focused on upland ecosystems, however, and far less is known about the dynamics of coastal regions [1,27].

Rs in coastal TAIs exhibit unique characteristics that distinguish it from other ecosystems due to specific environmental conditions and interactions within the land-ocean transitional zones. Rs in these environments can be influenced by the presence of halophytic plants adapted to tolerate high salinity [28]. Coastal transitional aquatic ecosystems receive nutrients from both land and sea, shaping a unique cycling process involving microbes, organic matter, nutrients, and phytoplankton interactions [29–31]. Factors such as organic matter availability and plant community composition affect soil respiration rates by influencing microbial activity, nutrient deposition from tidal waters, and root respiration interactions [32,33]. Moreover, different plant species have varying phenological patterns which affect the quantity and quality of organic matter inputs to the soil. Increased plant productivity may contribute more organic matter to the soil through root exudates and litterfall, leading to increased microbial activity and higher soil respiration rates [34]. Climate influences soil respiration directly through temperature and moisture. Warmer temperatures generally accelerate soil respiration rates by enhancing microbial activity and increasing rates of organic matter decomposition.

Moisture availability also plays a critical role, as soil moisture affects microbial activity and the availability of substrate for respiration [35,36]. Different land cover types (e.g., forests, grasslands, wetlands, urban areas) have distinct vegetation composition, organic matter inputs, and land management practices, all of which influence soil respiration [37]. Higher biodiversity often leads to increased productivity and a greater variety of organic inputs to the soil, which can enhance microbial diversity and activity, thereby impacting soil respiration rates [38]. Topographic features like slope, aspect, and elevation also can influence soil moisture, temperature, and nutrient availability, all of which can affect soil respiration rates [39,40]. Soil type, organic matter content, bulk density, nitrogen, pH, and microbial biomass are important factors influencing soil respiration [41]. For example, soils with higher organic matter content typically have higher respiration rates due to increased substrate availability for microbial decomposition [42]. Additionally, soil physical and chemical properties can interact with other environmental factors (e.g., plant roots, land use, and management practices) to modulate soil respiration dynamics [43].

Despite decades of research focused on coastal upland and wetland ecosystems and the boundary between them, there remains a large gap in our understanding of the processes by which climate, vegetation, topography, water, soil property, sediments, and microbes interact to drive spatial and temporal variation in carbon fluxes cycling across coastal TAIs [44]. The gap arises partially from the highly compressed spatial and temporal scales at which TAIs process change, which must be characterized by comparing the field measurements of fluxes into and out of the TAI ecosystem with surrounding landscape properties. The difficulty lies in the inability to effectively characterize the heterogeneity of coastal TAIs or quantify the material interactions between land and ocean [1], considering

the complex spatial variations in geomorphology, soil property, and vegetation communities [12]. This requires an extensive amount of spatially explicit data, which cannot be obtained solely through traditional field measurements.

Open source remote sensing and GIS products offer a feasible solution for studying coastal terrestrial-aquatic ecosystems, providing a comprehensive and synoptic view of dynamic TAI characteristics [45], for example, coastal wetland type identification [46–48], flooding area monitoring [49–51], geomorphology investigation [52–54], sediment concentration [55–57], coastal tree mortality [58–60], and coastal urbanization [61–63]. Remote sensing techniques have also been applied to estimate carbon fluxes and analyze the response of local environments to carbon fluxes in coastal ecosystems [64–69]. Overall, these open-source datasets offer considerable benefits for managing the sustainability and health of coastal regions that balance environmental, economic, and human needs. By leveraging data from multi-source, this study aims to characterize the spatial heterogeneity through zonation analysis based on clustering approach, as well as investigate the key environmental factors driving soil respiration. Coastal regions have unique characteristics that make them difficult to understand and model [1]. It is thus important to consider the specific characteristics and dynamics of each coastal ecosystem when applying these methods, as factors such as vegetation types, inundation, sediment composition, soil property, and climate variability can vary significantly across different regions.

In this study, we used multi-source remote sensing and GIS datasets to characterize above- and below-ground properties to investigate the spatial heterogeneity of the coastal terrestrial-aquatic ecosystem within the Chesapeake Bay (CPB) area and evaluate the major drivers of soil respiration. Being the largest estuary in the United States, CPB boasts a diverse array of flora and fauna, alongside various types of land use that intersect with human activity. A comprehensive assessment of the interplay between coastal catchment characteristics and soil respiration holds paramount importance in understanding carbon dynamics and forecasting the future course of atmospheric CO_2 concentrations. We employed a machine learning approach to identify the primary factors influencing soil respiration. Our hypotheses were that: (1) the regional catchment properties obtained from multi-source remote sensing products and GIS datasets enable statistical exploration of spatial heterogeneity and identification of spatial zones in similar ecological, topographic, and biochemical characteristics; and (2) the major driving factors affecting soil respiration exhibit variations within different sub-ecosystems in coastal TAIs. In addition, we aimed to validate whether the main driving factors identified by open-source remote sensing and GIS datasets are comparable to the field-based experimental findings.

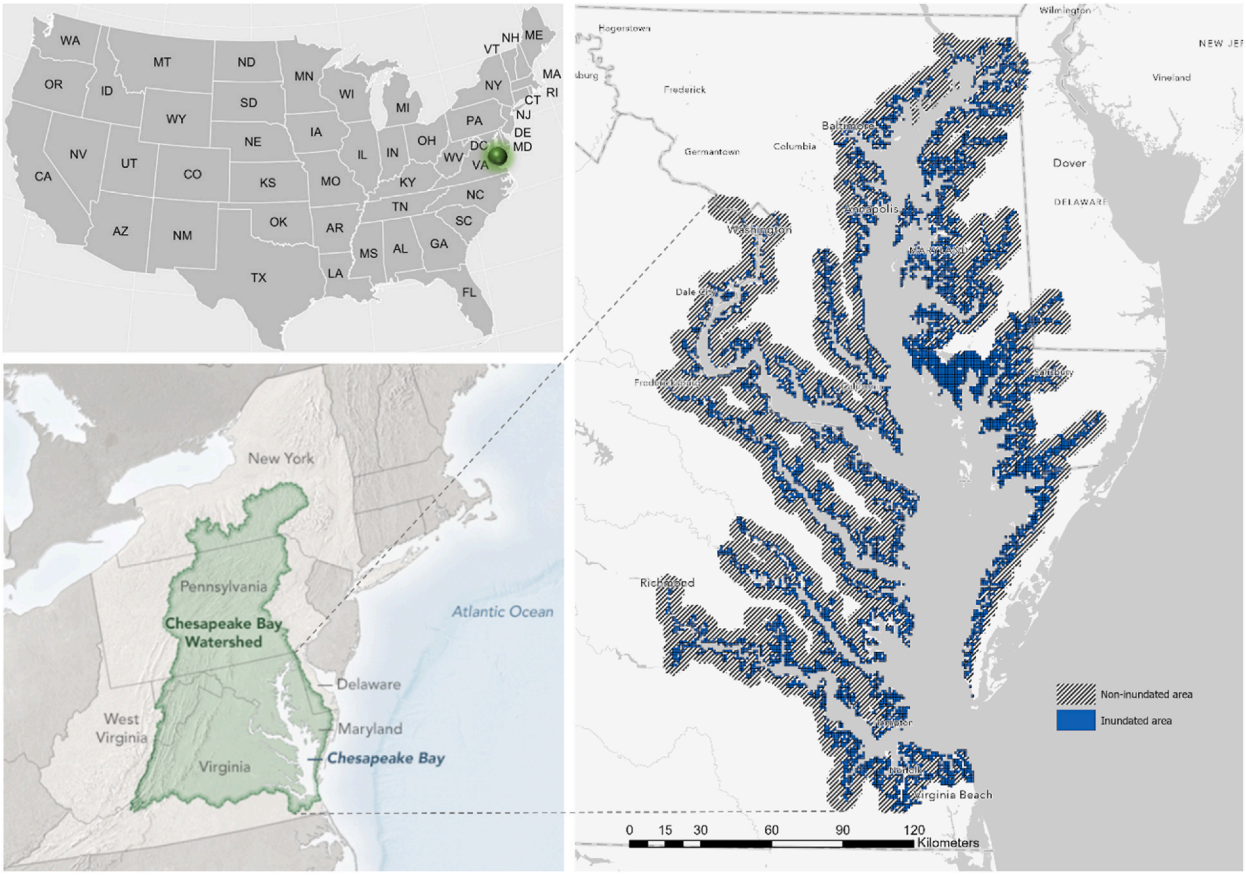

Fig. 1. Chesapeake Bay is situated in the Mid-Atlantic region and is mainly separated from the Atlantic Ocean by the Delmarva Peninsula, which encompasses sections of Maryland's Eastern Shore, Virginia's Eastern Shore, and Delaware. Inundated areas were derived from Ref. [74].

2. Study area

Our study area (centered at 37°57'45"N, 76°10'13"W) is located in the Chesapeake Bay (CPB) Watershed, a region along the Mid-Atlantic coast with a total area of 19,385 km^2 (Fig. 1). The CPB is the largest estuary in the United States and home to a wide variety of flora and fauna [70]. The predominant land use in the CPB is forest, but there are also areas with intensive agricultural practices and wetlands [71]. This region is characterized by a subtropical climate, featuring warm and humid summers, and cool to mild winters, stretching from the southern outlet of the Susquehanna River in Maryland to the mouth of the James River in Virginia. The average annual temperature in the region ranges from 13 °C in the north to 18 °C in the south, with hot (above 32 °C) summers and below-freezing winters. The region experiences an average of 1016–1270 mm of rainfall per year, with most of the precipitation falling between May and September [72]. The terrain of the CPB region varies from flat coastal plains to rolling hills and mountains, with the highest peak reaching over 1219 m. CPB is relatively shallow, with an average depth of 6.4 m and a maximum depth of 53 m, and its shallow depth and vast area make it sensitive to changes in land use and water quality [73].

3. Data and methods

Our research framework has three major steps: (i) data processing, (ii) determination of cluster number, and (iii) feature importance measurement. This paragraph provides a brief description of the workflow used in the study (Fig. 2). In step (i), a series of features were extracted and processed from multi-source remote sensing and GIS products, including carbon fluxes of soil respiration, vegetation phenological index, climate condition, land use and cover, Shannon diversity index, topography information, soil properties, inundation regions, and distance to shoreline (section 3.1). In step (ii), we determined the optimal cluster number by integrating unsupervised hierarchical clustering and post pairwise hypothesis test (section 3.2). In step (iii), we measured the feature importance

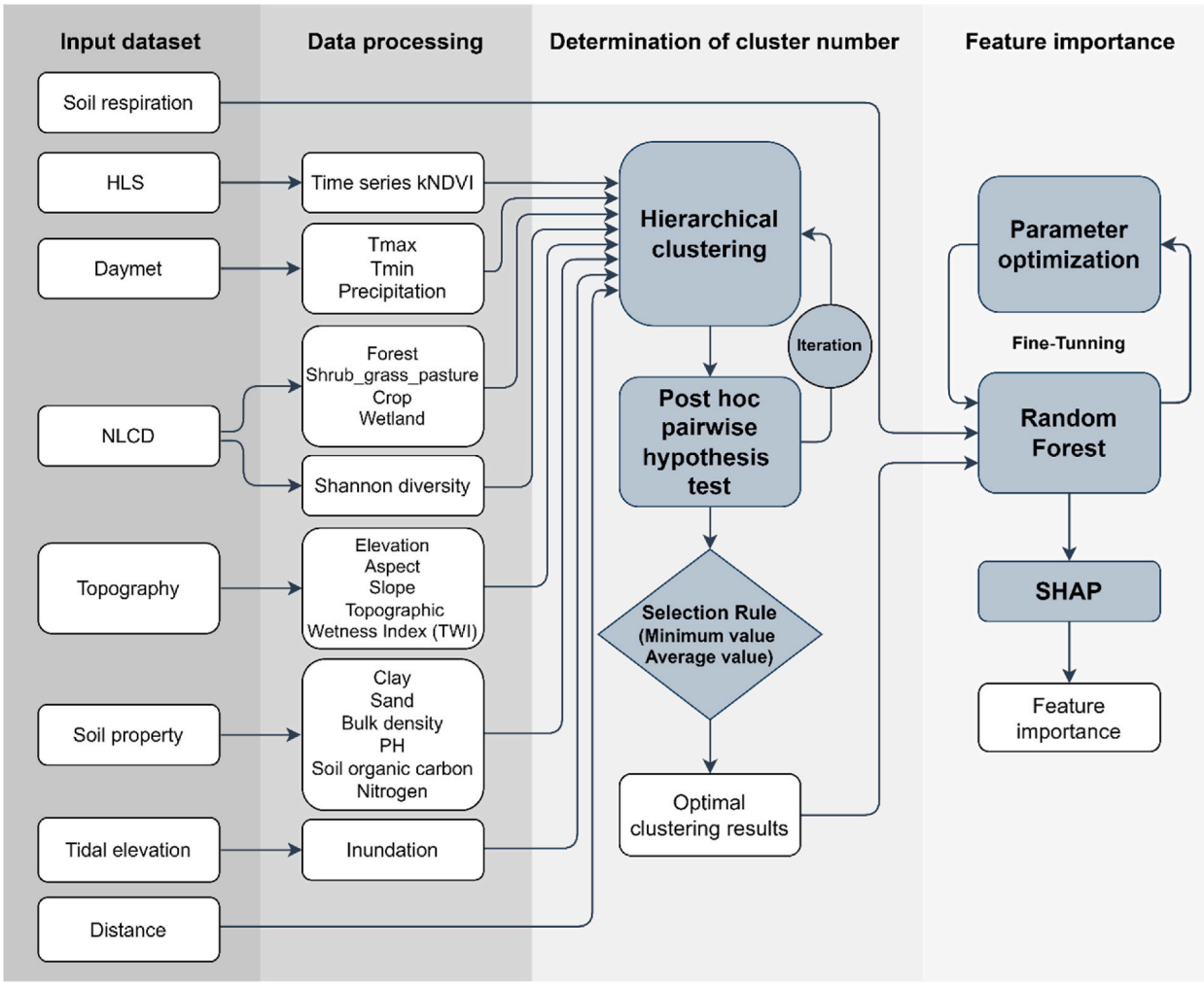

Fig. 2. Flowchart showing the processing steps in this study.

per each cluster using Random Forest regression and SHapley Additive exPlanations (SHAP) (section 3.3).

3.1. Data processing

3.1.1. Soil respiration data

In this study, soil respiration information was acquired from a generic global gridded estimate of annual soil respiration and soil heterotrophic respiration at 1 km spatial resolution (https://daac.ornl.gov/CMS/guides/SoilResp_HeterotrophicResp.html; [75]). This gridded estimation of soil respiration was carried out using a quantile regression forest model, the parameterization of which model utilized data from the global Soil Respiration Database Version 5 (SRDB-V5; [76]), covariates of mean annual temperature, seasonal precipitation, and vegetative cover. Particularly, the Global Soil Respiration Database (SRDB) is a publicly available dataset of soil respiration observations from peer-reviewed literature studies, initiated by Bond-Lamberty et al. [77] in 2010. The latest SRDB Version 5 is a compilation of in situ measurements from around the globe through 2017 (sample = 10,366). In CPB, we vectorized the gridded dataset in Ref. [26] and extended it 5 km inward along the coastline to create our regions of interest (Fig. 1).

3.1.2. Harmonized Landsat 8 and Sentinel-2 (HLS) imagery

We leveraged the Surface Reflectance Product of NASA's HLS (https://hls.gsfc.nasa.gov) to capture high-frequency temporal vegetation phenology. HLS data has a high temporal frequency of 3–4 days, which benefited from fusing the existing publicly available dataset of Landsat-8 and two Sentinel-2A and -2B satellites. The product of HLS involves a sequence of four processing steps, encompassing atmospheric correction and cloud masking, geometric resampling and geographic registration, bidirectional reflectance distribution function (BRDF) normalization, and band path adjustment. A comprehensive technical description of this product is presented in Ref. [78]. For this work, we used Version 1.4 of 30 m spatial resolution HLS data. A total of 2008 scenes for the year 2019 were downloaded and processed. We then calculated kNDVI and used it as a robust proxy for the vegetation productivity of our study area. kNDVI is a nonlinear generalization of NDVI and has proven to be a more accurate measure of terrestrial carbon source/sink dynamics and vegetation productivity [79].

$$kNDVI = \tanh\left(\left(\frac{NIR - Red}{2\sigma}\right)^2\right) \tag{1}$$

Where σ is a tunable length scale parameter intended to capture nonlinear sensitivity of NDVI to vegetation density, NIR is the near infrared band, and Red is the red band. Following the suggestion in Ref. [79], we used the generalization value of $\sigma = 0.5 \times (NIR + Red)$, which simplifies Eq. (1) to $kNDVI = tanh((NDVI)^2)$. Because kNDVI is designed to represent the biosphere for vegetated lands, we generated a vegetation mask using the 2019 National Land Cover Database (NLCD), finally, we calculated the fractional kNDVI value of the vegetated area in each 1 km grid in 2019.

3.1.3. Climate data

Climate factors are known to affect carbon dioxide flux from soils to the atmosphere as a result of autotrophic and heterotrophic belowground processes [80–82]. The climatic data used in this study were obtained from the Daymet (https://daymet.ornl.gov) gridded estimates of daily weather parameters. These estimates were generated by interpolating and extrapolating daily meteorological observations on a continuous surface dataset with a spatial resolution of 1 km, covering the Contiguous United States [83]. We extracted 1 km grid-level annual averages for minimum and maximum temperature and annual total precipitation in 2019 for subsequent analysis use.

3.1.4. National Land Cover Database (NLCD) data

The land cover dataset used in our study area was obtained from the National Land Cover Database (NLCD) for the year 2019 [84], which was procured from the Multi-Resolution Land Characteristics Consortium website (http://www.mrlc.gov). The NLCD dataset has a spatial resolution of 30 m and was generated using Landsat data as the primary input to develop a 16-class land cover classification scheme. In this study, biodiversity was quantified for inter-strata impact on soil respiration, Shannon Diversity Index was applied [85]:

$$\text{Shannon Diversity Index} = -\sum (P_i \times ln\ P_i) \tag{2}$$

Where P_i is the relative abundance of a species within a unit. Shannon Diversity Index = 0, when the grid contains only 1 patch type (i.e., no diversity). Shannon Diversity Index increases as the number of different patch types (i.e., patch richness) increases, and/or the proportional distribution of area among patch types becomes more equitable. We employed the Python implementation in the package PyLandStats (https://github.com/martibosch/pylandstats) to complete the Shannon Diversity Index procedure.

To further extract the land cover information in each 1 km grid unit, we aggregated the NLCD land cover into four main categories, namely forest (comprising deciduous forest, evergreen forest, and mixed forest), shrub/grass/pasture (including shrub, scrub, grasslands, and herbaceous areas), wetland (woody wetland, and emergent herbaceous wetland), and cropland. Ultimately, the areal proportion of specific land cover in each 1 km grid was calculated.

3.1.5. Topography data

To account for the heterogeneous topography, we utilized the 10 m high-resolution Digital Elevation Model (DEM) from the 3D Elevation Program (https://www.usgs.gov/3d-elevation-program; 3DEP). The 3DEP program is a collaborative effort among federal agencies, state/local governments, and tribal partners to collect and deliver high-quality, high-resolution elevation models for the USA through precise light detection and ranging (LiDAR) and interferometric synthetic aperture radar (InSAR) data [86]. From this data, we derived several topographic variables, including elevation, slope, aspect, and the topographic wetness index (TWI). The TWI provides insight into the impact of topography on local moisture availability and was computed as the natural logarithm of the ratio between the upslope contributing drainage area and the slope gradient of the grid cell [87]. The upslope contributing drainage area represents the accumulation of water flow from upstream areas.

3.1.6. Soil property data

This research utilized the US SoilGrid100 m maps to extract six types of soil properties, i.e., clay content, sand content, bulk density (BD), pH value, soil organic carbon (SOC), total nitrogen (TN), these datasets are publicly accessible through Penn State University repository (https://scholarsphere.psu.edu) or GitHub repository (https://github.com/aramcharan/US_SoilGrids100m). These soil property maps were developed using three national U.S. soil point datasets (NCSS Characterization Database, National Soil Information System, and Rapid Carbon Assessment), in combination with remotely sensed products and machine learning algorithms (Random Forest and Gradient Boosting). These soil property maps provide high-resolution spatial information for the Conterminous United States at 100-m spatial resolution for 7 standard soil depths (0, 5, 15, 30, 60, 100, and 200 cm) [88]. We calculated the mean value of each soil property across these seven depths in each 1 km grid for further analysis.

3.1.7. Tidal elevation data

Tidal inundation has a significant impact on soil respiration. We used a dataset of relative tidal marsh elevation maps, which provides maps of the elevation of coastal wetlands relative to tidal ranges for the Conterminous United States (CONUS) at 30 m resolution (https://daac.ornl.gov/CMS/guides/Coastal_US_Elevation_Data.html; [74]). These maps were developed using partial derivatives to compute the relative tidal elevation. The method involved normalizing the elevation of estuarine wetlands and adjacent palustrine wetlands to the tidal amplitude at mean high water (MHW). This process was applied to the wetlands that had a probability greater than 1 % of being below the mean higher high water spring (MHHWS) tide elevation layer crossing the USA's coastal regions and any wetlands classified as tidal in the National Wetland Inventory. Along with the relative tidal elevation, we identified the inundated region (see Fig. 1) and calculated the fraction of the inundated area for each 1 km grid for subsequent modeling.

3.2. Determination of cluster number

We used hierarchical agglomerative clustering (HAC; [89]), an unsupervised machine learning technique, to cluster input features and identify zones with similar characteristics in the CPB terrestrial aquatic ecosystem. This clustering method works by measuring the distance between pairs of observations and gradually merging them into larger clusters based on their similarity. The algorithm starts with each data point as a separate cluster and merges them based on increasing levels of similarity, forming a dendrogram that shows the hierarchical relationships between the clusters. We chose Ward's criterion as our distance measure, which minimizes the total

Table 1
Description of environmental factors used in analyses. In total, 21 factors were chosen to represent eight aspects of environmental conditions: vegetation phenology, climate, land cover, biodiversity, topography, soil property, relative tidal elevation, and distance to the shoreline.

Factor type	Factor name	Description	Resolution	Reference
Vegetation	kNDVI	Mean kernel Normalized Difference Vegetation Index	30 m	[79]
Climate	Tmax	Annual average maximum temperature	1 km	[83]
	Tmin	Annual average minimum temperature		
	Prcp	Total accumulated precipitation		
Land cover	Forest	Fraction of forest land	30 m	[84]
	Shrub_grass_pasture	Fraction of shrub/grass/pasture land		
	Crop	Fraction of cropland		
	Wetland	Fraction of wetland		
Biodiversity	Shannon_diversity	Mean Shannon diversity	30 m	[85]
Topography	Elevation	Mean elevation	10 m	[86,87]
	Aspect	Mean aspect		
	Slope	Mean slope		
	TWI	Mean topographic wetness index		
Soil property	Clay_mean	Mean clay content	100 m	[88]
	Sand_mean	Mean sand content		
	BD_mean	Mean bulk density		
	pH_mean	Mean pH value		
	SOC_mean	Mean soil organic carbon content		
	TN_mean	Mean total nitrogen		
Tidal level	Inundation	Fraction of inundated area	30 m	[64]
Distance	Distance	Euclidean distance from centroid of grid to shoreline		

variance within each cluster by merging pairs of clusters that result in the minimum variance. This method has been successful in previous studies on coastal TAIs [10,90].

We tested 21 features covering eight aspects of local environmental conditions that play an important role in soil respiration (Table 1, see data and pre-processing of the flowchart in Fig. 2 and section 3.1 for details). We implemented data standardization and Principal Component Analysis (PCA; cumulative explained variance >90 %) to prevent the model from being biased toward features with larger scales or ranges and make it more computationally efficient [91]. After performing hierarchical clustering, we conducted post hoc pairwise hypothesis tests to compare the mean differences between clusters to help us determine which clusters are significantly different and which ones are similar. For HAC, we used the Python implementation in the package Scikit-learn, and for post hoc pairwise hypothesis tests we used the specific Python package - scikit-posthocs (https://github.com/maximtrp/scikit-posthocs). We applied t-tests to make this pairwise comparison and determine the optimal clustering number in our study area. We defined the below criteria for the purpose of determining the optimal clustering number.

$$Ratio_{i,f} = \frac{Number\ of\ significant\ difference}{Total\ number\ of\ pairs} \tag{3}$$

Where *Ratio* represents the percentage of the number of significant differences to the total population, i represents the candidate value of cluster number from 3 to 21, f represents the input feature.

To determine the optimal number, the following criteria and requirements must be met: (i) The minimum value of the ratio must be greater than 0.80; (ii) The mean value of the ratio of all features must be the highest among all candidate values of cluster number [92].

3.3. Feature importance analysis

To identify environmental key drivers within each cluster, we performed a multivariate analysis and feature importance estimation using Random Forest regression and Shapley Additive exPlanations (SHAP) technique. Random Forest regression algorithm is an ensemble-learning algorithm that combines a large set of regression trees, which has been successfully applied in carbon flux studies [93,94]. In Random Forest regression, the algorithm begins by generating several bootstrap samples from the input training dataset. For each bootstrap sample, a decision tree is constructed by recursively splitting the data based on a set of conditions or restrictions. At each split, a random subset of input variables is considered for binary partitioning, which helps to reduce overfitting and increase model generalization. Once all the trees are constructed, predictions for a new observation are made by averaging the predictions of all the trees. Such an ensemble approach helps to reduce the impact of individual trees that may be biased or overfit to the training data. To develop a regression model using Random Forest, a set of hyper-parameters needs to be configured. These hyper-parameters are optimized by selecting the optimal values that produce the lowest error on the validation dataset. To efficiently search for the optimal hyper-parameter values, we employed a "random search" strategy (n_iter = 2000), which involved repeatedly training the Random Forest model using a random sample of all possible combinations of hyper-parameter values. This approach is particularly effective and greatly improves the efficiency of optimization when the model's performance is primarily influenced by only a subset of hyper-parameters [95]. To get a robust evaluation of model performance per cluster, we employ an 80/20 split and a 10-fold cross-validation technique. The details of the hyper-parameter optimization process are presented in Table 2.

Following the developed models per cluster, we utilized SHAP to interpret the feature importance in soil respiration projection. SHAP is a unified approach for explaining the output of any machine learning model by computing the contribution of each feature to the final prediction through the utilization of Shapley values [96]. The main idea behind SHAP is to use the concept of Shapley values from cooperative game theory to explain the output of a model. The Shapley value of a feature represents the expected marginal contribution of that feature to the prediction, considering all possible combinations of features, it quantifies the extent to which a particular feature influences the model's output while controlling for the influence of other features [97]. The feature importance was calculated as the mean absolute Shapley value (i.e., mean of |SHAP value|) using all samples as input. For Random Forest regression, we used the Python implementation in the package Scikit-learn, and for SHAP we used the specific Python package (https://github.com/slundberg/shap).

4. Results

4.1. Clustering

The results are presented in Fig. 3, where Fig. 3a depicts the trends observed in the minimum and mean ratios across the range of

Table 2
Hyper-parameters of Random Forest regression and corresponding value ranges for a random search strategy.

Model	Hyper-parameter	Candidate values
Random Forest Regressor	n_estimators	100, 200, 300, 400, 500, 600, 700, 800, 900, 1000, 1100, 1200
	max_depth	3, 6, 9, 12, 15, 18, 21
	min_samples_split	2, 4, 6, 8, 10, 12, 14, 18, 20, 22, 24, 26, 28, 30, 32, 34, 36, 38, 40
	min_samples_leaf	1, 3, 5, 7, 9, 11, 13, 15, 17, 19, 21
	max_features	'log2', 'sqrt', All

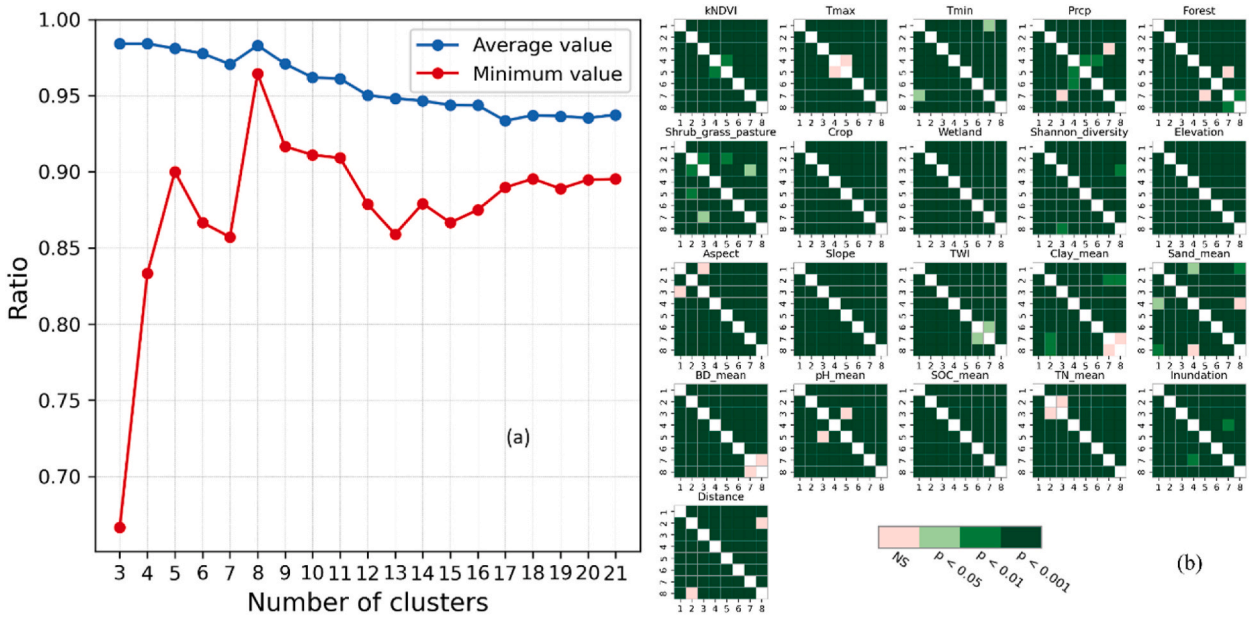

Fig. 3. (a) The minimum and mean ratios for which input features are pairwise significantly different for each number of clusters ($p < 0.05$); (b) Post hoc pairwise significance heatmap of each input feature for 8 clusters. NS stands for Not Significant.

cluster numbers (3–21), indicating that 8 clusters exhibited the most favorable results; Fig. 3b illustrates the outcomes of the post hoc pairwise hypothesis test, providing insights into the significant differences in means among the 21 environmental variables for the derived 8 clusters.

The analysis of the 21 environmental factors resulted in the identification of eight distinct clusters in the study area. The spatial distribution of these clusters is depicted in Fig. 4a, highlighting the variability across the region. Each cluster exhibits unique characteristics related to vegetation condition, topography, soil composition, and tidal level. Cluster 1 stands out with the highest Shannon diversity index, and represents a mixture of shrub, grass, pasture, and forest areas. Clusters 2 and 5 are primarily composed of croplands, but cluster 5 is distinguished by its high sand content and low clay content than cluster 2. Cluster 3 represents upland forested regions situated farthest from the shoreline in high elevation areas. Clusters 4 and 6 are associated with wetland environments, with cluster 6 exhibiting more pronounced inundation by tides. Cluster 6 also displays the highest soil organic content and total nitrogen, along with the lowest bulk density and sand content, compared to cluster 4. Cluster 7 represents dense plant-covered lands with high vegetation productivity (kNDVI) and is characterized by its proximity to the shoreline and the highest topographic wetness. Lastly, cluster 8 predominantly consists of urban and developed lands, with the highest land surface temperature recorded.

Boxplots of Fig. 5 demonstrate the details of the variability in each feature. To further understand the variation of soil respiration among the identified clusters, we generated individual boxplots (Fig. 4b) and pairwise *t*-test results (Fig. 4c) for each cluster, allowing for a comparison of their central tendencies and variability. We found that the mean values of Rs in cluster 1 and cluster 7, cluster 3 and cluster 5, as well as cluster 6 and cluster 8, were relatively close to each other (see Fig. 4c). These findings suggest that there may not be statistically significant differences in the mean Rs between these cluster pairs.

4.2. *Environmental drivers for soil respiration*

Random Forest regression model explained significant variation in carbon fluxes for all 8 clusters. However, the predictability of the model varied from cluster to cluster. Table 3 presents summary statistics obtained from Random Forest regression, indicating the quality of the regression model and the optimal settings used for each cluster. There is a significant variation in the R^2 and RMSE for the different clusters. Cluster 5 is the most predictable cluster, followed by Cluster 1. Cluster 7 is the least predictable. The optimal parameters for each cluster also vary. This means that there is no one-size-fits-all approach to modeling carbon fluxes. The optimal parameters varied depending on the specific cluster being modeled.

The average |SHAP| of all features was used to determine the primary driving factors per cluster. Clusters exhibited significant variation in their feature importance, suggesting the importance of different features in predicting carbon fluxes depends on the specific cluster being modeled (Fig. 6). The most important features for predicting soil carbon fluxes are generally related to climate, topography, and soil properties. The main factors vary from cluster to cluster, but some features are consistent across clusters, such as Tmax, Tmin, and Precipitation. Other factors, such as bulk density, clay content, sand content, and elevation, exhibit variations across clusters. Besides, when considering the whole area as domain, the feature importance analysis shows that while temperature and precipitation remain the most informative features, the information on soil texture (clay content), the local micro-topography (TWI), as well as land-use (cropland), becomes critical for the estimation of soil respiration. This is expected since these features provide

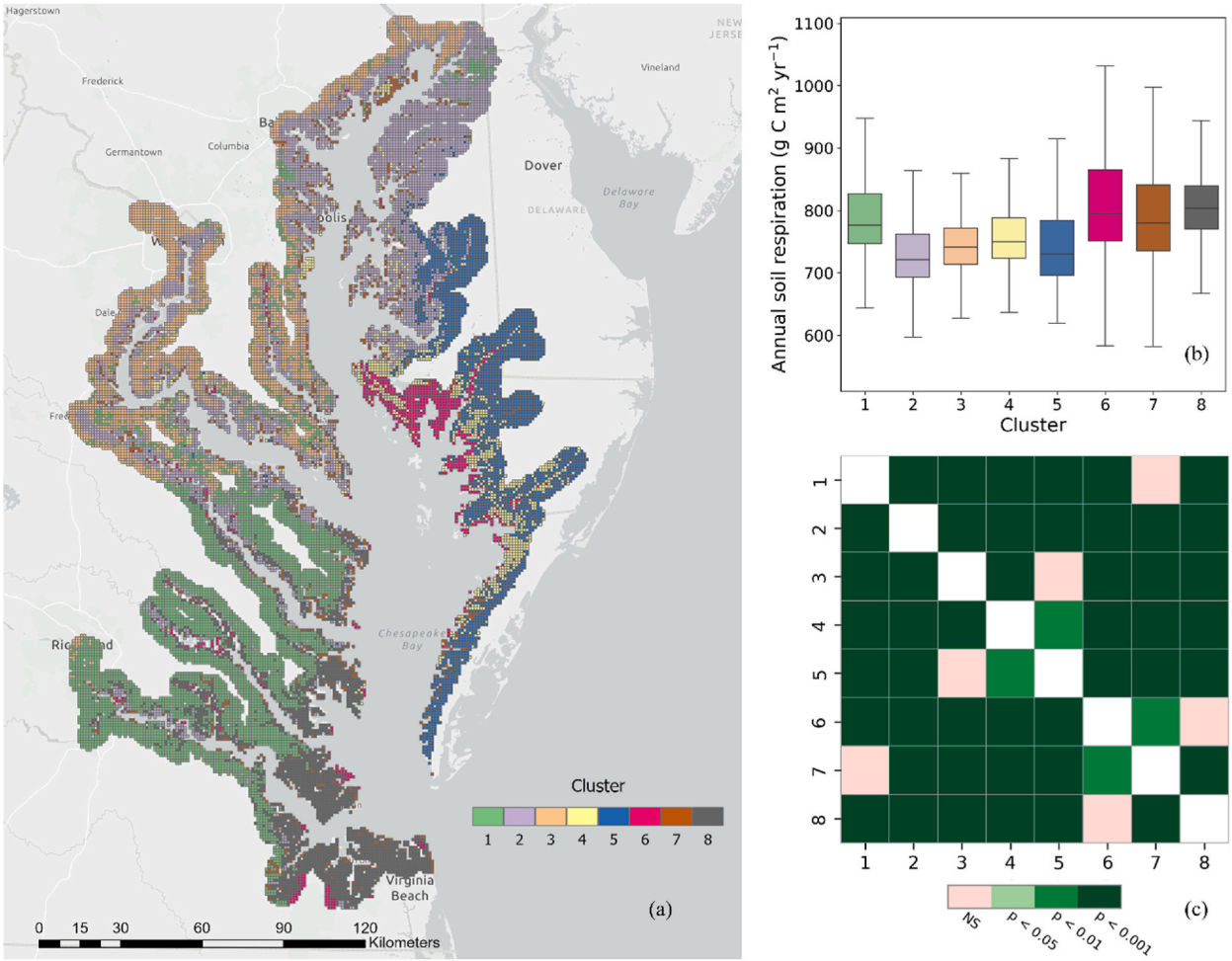

Fig. 4. (a) Spatial distribution of derived 8 clusters using hierarchical agglomerative clustering algorithm; (b) Boxplot of annual soil respiration per cluster; (c) Post hoc pairwise significance heatmap of soil respiration for 8 clusters. NS stands for Not Significant.

localized environmental information in a very heterogeneous ecosystem. These features indeed show high variability across the different clusters (see Fig. 5).

5. Discussion

5.1. Ecosystem variability

The coastal TAIs across the CPB are characterized by their remarkable diversity, encompassing a wide range of habitats within the transitional zones between land and ocean. The clustering presented herein allowed us to capture spatial variability in terms of vegetation, climate, land cover, biodiversity, topography, soil property, and inundation, as well as to identify 8 spatial regions with similar properties. Such spatial variability is likely due to differences in the structure, function, and composition of the coastal TAI ecosystems [98,99]. Topographic metrics (elevation and slope) and relative tidal elevation influence the spatial distribution and connectivity of wetland land cover. These wetland regions were close to shoreline, in low-lying lands and with high soil organic carbon content. This is primarily due to the accumulation of dead plant material, known as peat, in waterlogged and oxygen-deprived environments [100,101].

Forested lands are furthest away from the shoreline with the highest elevation in upland regions. These forested lands are often mixed with shrubs, grass, and pasture, which introduced structural complexity and increased species heterogeneity. This high species diversity in vegetation structure further provides varied niches and habitats for different plant species, leading to higher species richness and ecological interactions [102].

Most of the croplands are on the eastern shore of the CPB, and varying soil properties in these zones can be crucial for agricultural activities or habitat provisioning for certain crop types. For example, some of the crops commonly grown in this area: corn (maize) and soybeans can tolerate lower clay content and higher sand content in the soil [103,104]; crops with deep and thick root systems, such as

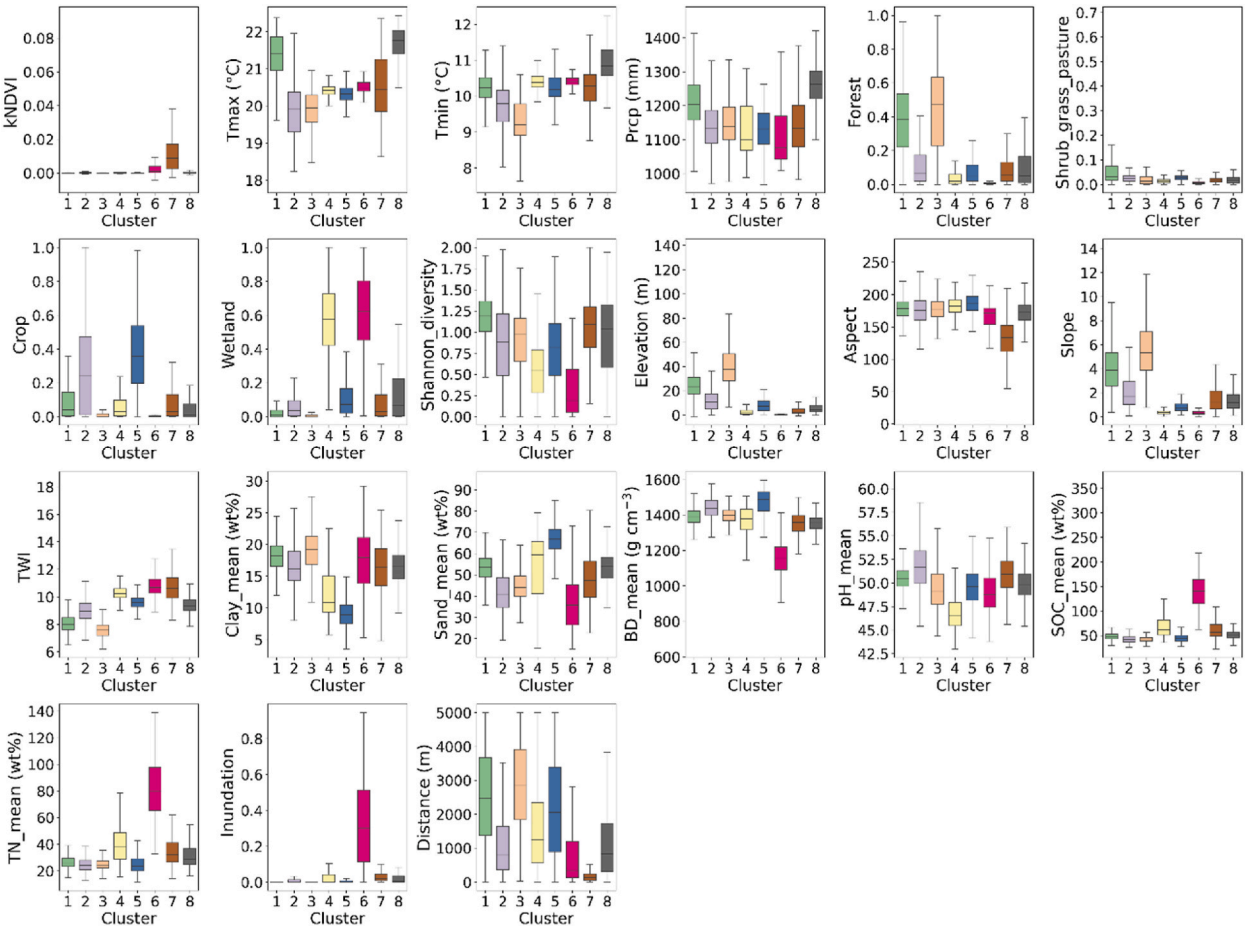

Fig. 5. Boxplots of input features for each cluster.

Table 3
Summary statistics per cluster and the whole area derived from Random Forest regressions and relative optimal parameters.

Cluster #	1	2	3	4	5	6	7	8	All
Sample size	4571	4426	2832	971	2491	721	988	2386	19,386
R^2	0.83	0.76	0.76	0.85	0.94	0.85	0.61	0.62	0.84
RMSE	27.98	30.88	41.82	36.92	23.89	36.93	46.54	31.76	29.74
n_estimators	900	400	300	800	1200	500	1100	900	300
max_depth	18	18	18	18	15	18	18	18	21
min_samples_split	4	2	5	2	4	6	2	3	2
min_samples_leaf	1	1	1	1	1	1	1	1	1
max_features	All	All	All	All	All	All	All	All	All

sunflowers, canola, and deep-rooted legumes like alfalfa, can tolerate higher bulk density soils [105,106]. High land surface temperatures were observed in urban and developed areas. These areas often have limited green spaces and sparse plant cover compared to natural areas. Trees, plants, and green spaces help regulate temperatures through evapotranspiration and shading. In their absence, developed areas experience a lack of natural cooling mechanisms, resulting in elevated land surface temperatures [107].

While this study provides a spatially explicit representation of TAI's soil respiration variability, the carbon fluxes of coastal regions are less well understood in general [1]. It is essential to recognize that such analyses are specific to CPB and uncertainties may be introduced due to the spatial scale of investigation and the availability of ready-to-use products in the process of sub-ecosystem delineation and primary driving factor determination. In our study, we found that Tmax, Tmin, and Precipitation exerted considerable influence on the variability of soil respiration at a large regional scale. However, these differences may not be as significant at smaller spatial scales, making it challenging to accurately predict soil respiration solely based on these factors. Additionally, the presence of dissolved organic carbon (DOC), nitrate, and ammonia concentrations in soil can also significantly influence microbial activity and respiration processes [108–110].

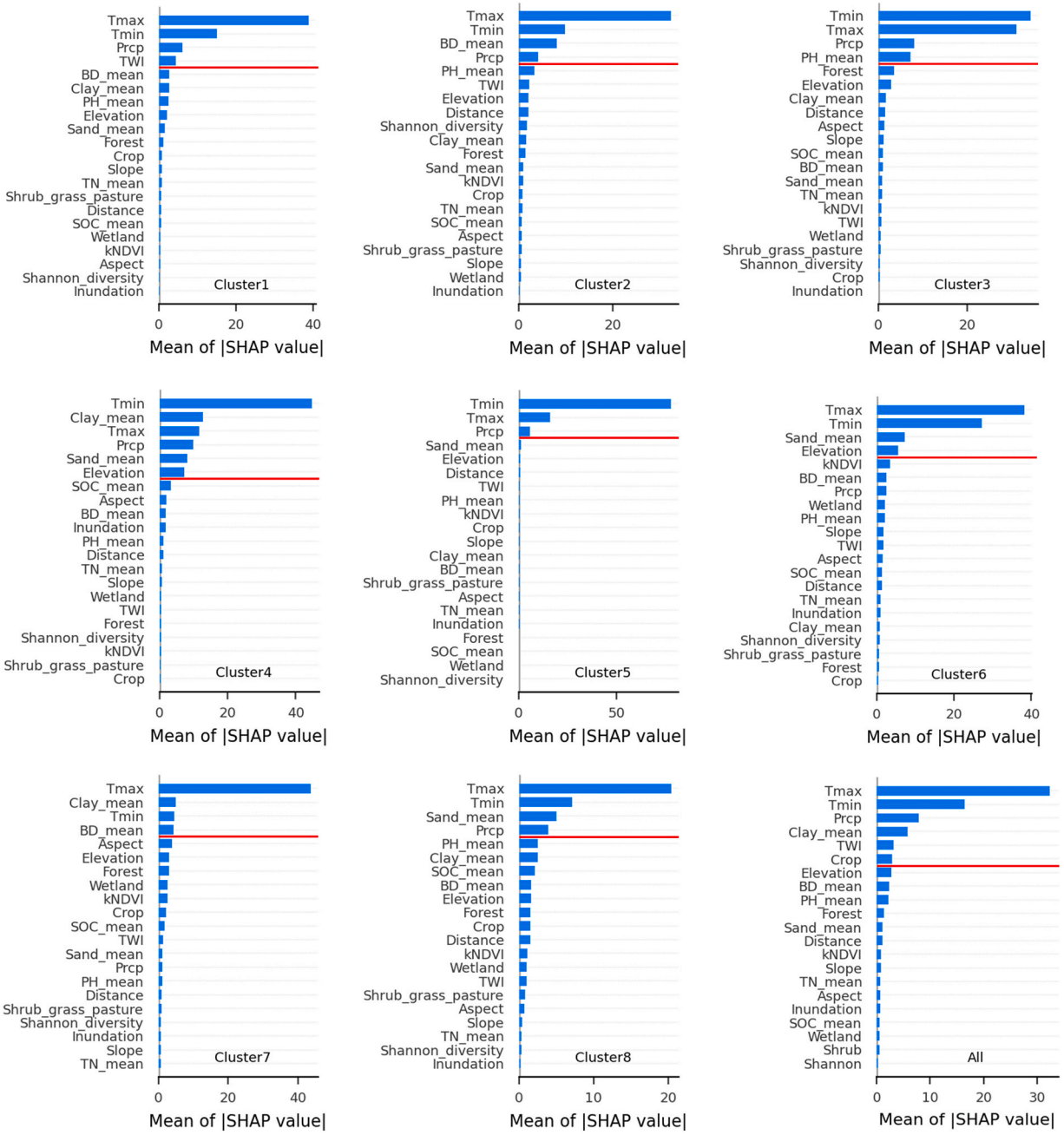

Fig. 6. Feature importance for each cluster and the whole area in estimating soil respiration was determined by integrating Random Forest regression and SHAP (SHapley Additive exPlanations). The |SHAP| of features above the red line is greater than the average |SHAP| of all features. |SHAP| represents the absolute value of SHAP. (For interpretation of the references to colour in this figure legend, the reader is referred to the Web version of this article.)

On the other hand, TAI ecosystems, such as CPB, show very heterogeneous ecosystem properties, which are difficult to model. Through clustering analysis, we were able to understand the spatial heterogeneity and identify specific coastal zones characterized by distinct environmental characteristics. These zones effectively capture the spatial heterogeneity that exists across the CPB, represented by the diverse range of co-varying land cover, plant productivity, topographic properties, and tidal effects, highlighting the inherent relationship between environmental factors and ecological processes. It is noteworthy that our approach sets itself apart from other studies conducted in the CPB region that often are limited to specific subsets of the TAI system by field measurement [111–113], we integrated multi-source remote sensing/GIS products and machine learning algorithms to provide a spatially explicit of varied ecosystem variability. Furthermore, the determination of the optimal number of clusters is achieved through an iterative procedure

involving post hoc pairwise hypothesis tests, a step that can potentially yield varying cluster numbers and correspondingly distinct coastal sub-regions in different study cases, which are also based on the varied available remote sensing/GIS products.

5.2. Impact of environmental properties on soil respiration

Climate factors (maximum and minimum temperature) make a significant contribution to soil respiration crossing ecosystems due to their direct and indirect influences on key biological and physical processes that drive soil respiration. Soil respiration is primarily driven by microbial activity, particularly by soil microorganisms such as bacteria and fungi [32]. Microbes are highly temperature-sensitive, and their metabolic processes are directly affected by temperature [114,115]. Warmer temperatures generally accelerate microbial activity, enzymatic reactions, and metabolic processes, leading to increased decomposition of organic matter and higher rates of soil respiration [116]. As a result, higher maximum and minimum temperatures provide more favorable conditions for microbial respiration, resulting in elevated soil respiration rates. Additionally, precipitation was found to have an impact on all vegetated lands, such as the lands of forests, shrubs, grass, crops, and woody wetlands. Precipitation influences soil respiration indirectly by affecting soil moisture and substrate availability. Adequate moisture levels are essential for microbial activity and the availability of dissolved organic carbon in the soil [117]. Precipitation also plays a role in the water-air balance within the soil. Excessive precipitation can saturate the soil, leading to poor aeration and reduced oxygen availability [118]. In such conditions, anaerobic respiration processes dominate, resulting in lower soil respiration rates. Conversely, moderate precipitation levels maintain optimal soil moisture and a well-aerated environment, facilitating aerobic respiration and higher soil respiration rates [119]. Our results are consistent with the findings of Najjar et al. [120] for the same study area, who found that soil CO_2 efflux was strongly regulated by both changes in precipitation and temperature.

In addition to temperature and rainfall, we observed differences in other major drivers between clusters, which may be attributed to variations in soil properties and topography in each region. The mixture, consisting of shrubs, grass, pasture, and forest regions, exhibited high species diversity (cluster 1). In these areas, TWI (topographic wetness index; Table 1) is another major driving factor apart from temperature and precipitation. The presence of different vegetation types in these mixed areas has different strategies for water uptake, water retention, and water loss, suggesting varying water requirements and adaptations to moisture conditions [121, 122]. In the areas with higher TWI and increased water accumulation potential, soil moisture levels may remain relatively high, creating favorable conditions for microbial respiration. Hopple et al. [123] conducted a field study in the Muddy Creek (a stream draining into an arm of the CPB) and demonstrated topography is a dominant control in the mixed forested land, where the topographic gradients are highly correlated with variability of Rs. The varying elevation gradients result in some measurement points draining faster than others, creating substantial differences in soil water content within the measured plots, these differences in soil moisture in turn lead to strong differences in soil respiration [124]. Thus, TWI helps capture the influence of terrain characteristics on water availability and movement, for a better exploration of soil respiration [125].

In croplands with high clay content and low sand content (cluster 2), bulk density plays a significant role in influencing soil respiration. In CPB, over one-quarter of the land is devoted to agricultural practices, some agricultural practices—including over-irrigating farmland, over-tilling soil, and over-applying fertilizers and pesticides —can break up soil structure, reducing the size and number of macropores and increasing bulk density, then in turn, affect the rate of soil respiration [126,127]. In these croplands, the compacted soil structure (higher bulk density) can limit the movement of air and gas exchange. As a result, oxygen availability in the root zone may be reduced. When oxygen availability is limited, microbial activity and subsequent soil respiration rates may be hindered. In addition, high clay content soils have high water-holding capacity due to their small particle size and greater surface area [128]. However, when the soil is compacted, water movement through the soil can be impeded. Poor water drainage and increased water saturation can lead to oxygen depletion in the soil, creating anaerobic conditions that are less favorable for soil respiration [129]. Our finding (Fig. 4b) also confirmed that the agricultural land has lower soil respiration than other land in the CPB region. Further exploration is warranted due to the substantial spatial variations in soil respiration observed across various types of croplands [130]. These differences primarily stem from diverse vegetation types and varied management practices, including fertilization, tillage, irrigation, and crop density [131–133]. Understanding these disparities is imperative for accurately assessing carbon budgets and devising effective strategies to mitigate the impacts of agricultural practices on climate change.

Soil pH affects soil respiration of the forest ecosystem (cluster 3). The soil pH level can interplay with factors like temperature, moisture and organic matter, affecting soil respiration [134]. In a study by Vanhala et al. [135] in the forest terrains, when assessing soil respiration rates at a steady temperature of 14 °C, both moisture and pH play a regulatory role. However, when the moisture level remains consistent at 60 % of its water-holding capacity, the primary factors affecting soil respiration are organic matter content and soil pH. Additionally, the forested land is often covered by dense fallen leaves. As the leaves decompose, organic acids are released, which can lower the soil pH near the litter layer. The process of leaf litter decomposition and the release of organic acids contribute to the complex interactions between organic matter, pH, microbial activity, and soil respiration in forest ecosystems [136].

Soil sand content and elevation both affect wetland soil respiration, but the presence of higher clay content has a stronger influence in non-inundated wetlands (cluster 4) than in tidal inundation wetlands (cluster 6). Non-inundated wetlands with higher clay content may provide more favorable conditions for microbial groups and enhance nutrient retention and availability, which can promote microbial activity and facilitate decomposition processes, leading to increased soil respiration rates [137]. While in the inundated wetland, Morrissey et al. [138] further reported that soil salinity also presented a strong correlation with both microbial activity composition and decomposition rates across a range of tidal wetlands from freshwater to oligohaline of the west CPB region in Virginia. We also found the dense plant-covered lands (cluster 7) and urban/developed lands (cluster 8) presented varied primary drivers. Soil clay content and bulk density are the driving factors in dense plant regions, while sand content is important in urban/developed areas.

In dense plant areas, soil clay content and bulk density probably contribute to soil respiration by enhancing water retention, maintaining favorable moisture conditions, and providing a suitable habitat for microorganisms involved in decomposition processes [139]. Conversely, in urban/developed lands, higher soil sand content resulting from human activities like construction and compaction can lead to reduced water-holding capacity and limited soil moisture availability [140]. This, in turn, hampers microbial activity and lowers soil respiration rates. Such anthroponomic activities-induced variations in soil characteristics result in significant spatial heterogeneity in soil respiration. Bettez and Groffman [141] found that, in the Baltimore City of CPB, highly developed forest areas and developed herbaceous areas had lower soil respiration rate compared to the undeveloped area.

The extent to which these findings are common to other coastal ecosystems is uncertain as soil respiration rates are critically dependent on local biogeochemical conditions, climate zones, topographic attributes, land-use change, and availability of datasets. The localized catchment characteristics of different coastal TAIs may thus have varying impacts on soil CO_2 efflux. For example, in a coastal forested wetland study in North Carolina of the US, soil respiration is highly impacted by flooding stage and water table depth, resulting in seasonal hysteresis in the Rs-soil temperature relationship [142]. Chen et al. [143] reported that seawater intrusion due to sea level rise reduced soil carbon emissions from freshwater wetlands in the Yellow River estuarine delta of China. The transformation of land use may significantly impact the ecological, topographic, and biochemical features within TAIs, warranting further investigation into its effects on soil respiration [144]. Nevertheless, the developed framework presented in this study offers the opportunity to bring together different data streams and characterize the spatial heterogeneity driving the ecosystem processes and therefore can be used to perform more in-depth investigation for specific case studies.

6. Conclusion

This study investigates the spatial clusters of similar ecological, topographic, and biochemical characteristics in coastal TAIs, and highlights the utility of open-source remote sensing and GIS products for spatially explicit monitoring and evaluation of driving soil CO_2 emission at the landscape scale. The characteristics of catchment properties enable the detection of spatial heterogeneity and variability within coastal terrestrial-aquatic ecosystems. Soil respiration in CPB's various sub-ecosystems was found to be influenced by maximum and minimum temperatures. Precipitation was observed to exert a significant influence on vegetated lands. In addition to climate factors, soil properties, and topographic attributes also act as the additional primary driving factors, although they demonstrate variances across different sub-ecosystems. Thus, integrating open source remote sensing and GIS products enables the spatially exhaustive assessment of multiple parameters simultaneously, which facilitates the delineation of the spatial heterogeneity and identification of the main driving factors of the different ecosystems of TAIs. Our study illustrates an effective way of using multi-source remote sensing and GIS products to understand the coastal soil respiration processes by which climate, soil property, topography, and vegetation drive spatial variability in carbon dynamics, which ensures our continued contribution to global carbon exchange and climate change mitigation efforts and actions.

Data availability

Publicly available datasets used in this study include: soil respiration grid (https://daac.ornl.gov/CMS/guides/SoilResp_HeterotrophicResp.html), Harmonized Landsat 8 and Sentinel-2 (HLS) imagery (https://hls.gsfc.nasa.gov), Daymet climate dataset (https://daymet.ornl.gov), National Land Cover Database (NLCD) dataset (http://www.mrlc.gov), Digital Elevation Model (DEM) from the 3D Elevation Program (https://www.usgs.gov/3d-elevation-program), US SoilGrid100 m maps (https://github.com/aramcharan/US_SoilGrids100m), Relative Tidal Marsh Elevation Maps (https://daac.ornl.gov/CMS/guides/Coastal_US_Elevation_Data.html). The data that support the findings of this study can be obtained from https://doi.org/10.15485/2326012. Source Python code are available at https://github.com/yhe-rs/hac-rf-shap.git.

CRediT authorship contribution statement

Yinan He: Writing – review & editing, Writing – original draft, Visualization, Validation, Methodology, Conceptualization, Data curation, Formal analysis. **Ben Bond-Lamberty:** Writing – review & editing, Resources, Funding acquisition. **Allison N. Myers-Pigg:** Writing – review & editing. **Michelle E. Newcomer:** Writing – review & editing. **Joshua Ladau:** Writing – review & editing. **James R. Holmquist:** Writing – review & editing. **James B. Brown:** Writing – review & editing. **Nicola Falco:** Writing – review & editing, Project administration, Methodology, Funding acquisition, Conceptualization.

Declaration of competing interest

The authors declare that they have no known competing financial interests or personal relationships that could have appeared to influence the work reported in this paper.

Acknowledgments

This research was supported by COMPASS-FME, a multi-institutional project supported by the U.S. Department of Energy, Office of Science, Biological and Environmental Research as part of the Environmental System Science Program. The Lawrence Berkeley National Laboratory operates for DOE under U.S. Department of Energy Award No. DE-AC02-05CH11231. We thank numerous

contributors for providing vital field, laboratory support, and thoughtful feedback in this study.

References

[1] N.D. Ward, J.P. Megonigal, B. Bond-Lamberty, V.L. Bailey, D. Butman, E.A. Canuel, H. Diefenderfer, N.K. Ganju, M.A. Goñi, E.B. Graham, C.S. Hopkinson, Representing the function and sensitivity of coastal interfaces in Earth system models, Nat. Commun. 11 (2020) 2458.
[2] J.P. Gattuso, M. Frankignoulle, R. Wollast, Carbon and carbonate metabolism in coastal aquatic ecosystems, Annu. Rev. Ecol. Evol. Syst. 29 (1998) 405–434.
[3] G.E. Likens, F.H. Bormann, Linkages between terrestrial and aquatic ecosystems, Bioscience 24 (1974) 447–456.
[4] A. Marion, V. Nikora, S. Puijalon, T. Bouma, K. Koll, F. Ballio, S. Tait, M. Zaramella, A. Sukhodolov, M. O'Hare, G. Wharton, Aquatic interfaces: a hydrodynamic and ecological perspective, J. Hydraul. Res. 52 (2014) 744–758.
[5] M.E. Newcomer, A.J.M. Kuss, T. Ketron, A. Remar, V. Choksi, J.W. Skiles, Estuarine sediment deposition during wetland restoration: a GIS and remote sensing modeling approach, Geocarto Int. 29 (2014) 451–467.
[6] S.E. Tank, J.B. Fellman, E. Hood, E.S. Kritzberg, Beyond respiration: controls on lateral carbon fluxes across the terrestrial-aquatic interface, Limnol. Oceanogr. 3 (2018) 76–88.
[7] A. Sengupta, J. Indivero, C. Gunn, M.M. Tfaily, R.K. Chu, J. Toyoda, V.L. Bailey, N.D. Ward, J.C. Stegen, Spatial gradients in the characteristics of soil-carbon fractions are associated with abiotic features but not microbial communities, Biogeosciences 16 (2019) 3911–3928.
[8] L.S. Tan, Z.M. Ge, S.H. Li, K. Zhou, D.Y. Lai, S. Temmerman, Z.J. Dai, Impacts of land-use change on carbon dynamics in China's coastal wetlands, Sci. Total Environ. 890 (2023) 164206.
[9] D.S. Baldwin, A.M. Mitchell, The Effects of Drying and Re-flooding on the Sediment and Soil Nutrient Dynamics of Lowland River–Floodplain Systems: a Synthesis, Regul. Rivers Res. Manag. 16 (5) (2000) 457–467.
[10] M.E. Newcomer, S.S. Hubbard, J.H. Fleckenstein, U. Maier, C. Schmidt, M. Thullner, C. Ulrich, N. Flipo, Y. Rubin, Influence of hydrological perturbations and riverbed sediment characteristics on hyporheic zone respiration of CO2 and N2, J. Geophys. Res. Biogeosci. 123 (2018) 902–922.
[11] L. Zhang, Y. Li, X. Sun, J.M. Adams, L. Wang, H. Zhang, H. Chu, More robust Co-occurrence patterns and stronger dispersal limitations of bacterial communities in wet than dry seasons of riparian wetlands, mSystems 8 (2) (2023) e0118722.
[12] L. Enguehard, N. Falco, M. Schmutz, M.E. Newcomer, J. Ladau, J.B. Brown, L. Bourgeau-Chavez, H.M. Wainwright, Machine-learning functional zonation approach for characterizing terrestrial–aquatic interfaces: application to lake erie, Rem. Sens. 14 (2022) 3285.
[13] W.J. Cai, Estuarine and coastal ocean carbon paradox: CO2 sinks or sites of terrestrial carbon incineration? Ann. Rev. Mar. Sci 3 (2011) 123–145.
[14] C. Nellemann, E. Corcoran, C.M. Duarte, L. Valdés, C. De Young, L. Fonseca, G. Grimsditch, Blue Carbon: A Rapid Response Assessment, United Nations Environment Programme, 2009. GRID–Arendal.
[15] J. Hauck, M. Zeising, C. Le Quéré, N. Gruber, D.C. Bakker, L. Bopp, T.T.T. Chau, Ö. Gürses, T. Ilyina, P. Landschützer, A. Lenton, Consistency and challenges in the ocean carbon sink estimate for the global carbon budget, Front. Mar. Sci. 7 (2020) 571720.
[16] L. Pendleton, D.C. Donato, B.C. Murray, S. Crooks, W.A. Jenkins, S. Sifleet, C. Craft, J.W. Fourqurean, J.B. Kauffman, N. Marbà, P. Megonigal, Estimating global "blue carbon" emissions from conversion and degradation of vegetated coastal ecosystems, PLoS One 7 (2012) e43542.
[17] D.M. Alongi, Coastal Ecosystem Processes, CRC Press, Cambridge, MA, 1998.
[18] R.G. Wetzel, Land-water interfaces: metabolic and limnological regulators, Verh. Int. Ver. Limnol. 24 (1990) 6–24.
[19] T.D. Colmer, T.J. Flowers, Flooding tolerance in halophytes, New Phytol. 179 (2008) 964–974.
[20] J. Holden, Peatland hydrology and carbon release: why small-scale process matters, Philos. Trans. R. Soc. A. 363 (2005) 2891–2913.
[21] S. Emerson, Organic carbon preservation in marine sediments, in: E.T. Sundquist, W.S. Broecker (Eds.), The Carbon Cycle and Atmospheric CO2: Natural Variations Archean to Present, Am. Geophys. Union, Washington, D.C., 1985, pp. 78–87.
[22] C. Smeaton, W.E. Austin, Sources, sinks, and subsidies: terrestrial carbon storage in mid-latitude fjords, J. Geophys. Res. Biogeosci. 122 (2017) 2754–2768.
[23] M. Adachi, A. Ito, S. Yonemura, W. Takeuchi, Estimation of global soil respiration by accounting for land-use changes derived from remote sensing data, J. Environ. Manag. 200 (2017) 97–104.
[24] J.W. Raich, A. Tufekcioglu, Vegetation and soil respiration: correlations and controls, Biogeochemistry 48 (2000) 71–90.
[25] J.P.E. Anderson, Soil respiration, in: A.L. Page (Ed.), Methods of Soil Analysis, Part 2. Chemical and Microbiological Properties, Soil Science Society of America, Madison, WI, 1982, pp. 837–871.
[26] E. Stell, D. Warner, J. Jian, B. Bond-Lamberty, R. Vargas, Spatial biases of information influence global estimates of soil respiration: how can we improve global predictions? Global Change Biol. 27 (2021) 3923–3938.
[27] B. Bond-Lamberty, A. Ballantyne, E. Berryman, E. Fluet-Chouinard, J. Jian, K.A. Morris, A. Rey, R. Vargas, Twenty years of progress, challenges, and opportunities in measuring and understanding soil respiration, J. Geophys. Res. Biogeosci. 129 (2) (2024) e2023JG007637.
[28] W. Qu, J. Li, G. Han, H. Wu, W. Song, X. Zhang, Effect of salinity on the decomposition of soil organic carbon in a tidal wetland, J. Soils Sediments 19 (2019) 609–617.
[29] Y. Cheng, V.N. Bhoot, K. Kumbier, M.P. Sison-Mangus, J.B. Brown, R. Kudela, M.E. Newcomer, A novel random forest approach to revealing interactions and controls on chlorophyll concentration and bacterial communities during coastal phytoplankton blooms, Sci. Rep. 11 (2021) 19944.
[30] D.B. Lewis, J.A. Brown, K.L. Jimenez, Effects of flooding and warming on soil organic matter mineralization in Avicennia germinans mangrove forests and Juncus roemerianus salt marshes, Estuar. Coast Shelf Sci. 139 (2014) 11–19.
[31] A.E. Sutton-Grier, J.K. Keller, R. Koch, C. Gilmour, J.P. Megonigal, Electron donors and acceptors influence anaerobic soil organic matter mineralization in tidal marshes, Soil Biol. Biochem. 43 (2011) 1576–1583.
[32] W. Cheng, Y. Kuzyakov, Root effects on soil organic matter decomposition, in: S. S. Wright, R. Zobel (Eds.), Roots and Soil Management: Interactions between Roots and the Soil, Agronomy Monograph No. 48, American Society of Agronomy, Madison, Wisconsin, USA, 2005, pp. 119–143.
[33] D.B. Metcalfe, R.A. Fisher, D.A. Wardle, Plant communities as drivers of soil respiration: pathways, mechanisms, and significance for global change, Biogeosciences 8 (2011) 2047–2061.
[34] G. Han, Q. Xing, Y. Luo, R. Rafique, J. Yu, N. Mikle, Vegetation types alter soil respiration and its temperature sensitivity at the field scale in an estuary wetland, PLoS One 9 (3) (2014) e91182.
[35] G. Han, B. Sun, X. Chu, Q. Xing, W. Song, J. Xia, Precipitation events reduce soil respiration in a coastal wetland based on four-year continuous field measurements, Agric. For. Meteorol. 256 (2018) 292–303.
[36] O.R. Anderson, Soil respiration, climate change and the role of microbial communities, Protist 162 (2011) 679–690.
[37] X. Song, Y. Zhu, W. Chen, Dynamics of the soil respiration response to soil reclamation in a coastal wetland, Sci. Rep. 11 (2021) 1–14.
[38] C. Chen, H.Y. Chen, X. Chen, Z. Huang, Meta-analysis shows positive effects of plant diversity on microbial biomass and respiration, Nat. Commun. 10 (2019) 1332.
[39] M. Sommerkorn, Micro-topographic patterns unravel controls of soil water and temperature on soil respiration in three Siberian tundra systems, Soil Biol. Biochem. 40 (2008) 1792–1802.
[40] G. Miao, A. Noormets, J.C. Domec, M. Fuentes, C.C. Trettin, G. Sun, S.G. McNulty, J.S. King, Hydrology and microtopography control carbon dynamics in wetlands: implications in partitioning ecosystem respiration in a coastal plain forested wetland, Agric. For. Meteorol. 247 (2017) 343–355.
[41] H.E. Steinmuller, K.M. Dittmer, J.R. White, L.G. Chambers, Understanding the fate of soil organic matter in submerging coastal wetland soils: a microcosm approach, Geoderma 337 (2019) 1267–1277.
[42] A. Gershenson, N.E. Bader, W. Cheng, Effects of substrate availability on the temperature sensitivity of soil organic matter decomposition, Global Change Biol. 15 (2009) 176–183.

[43] J. Li, L. Pu, M. Zhu, J. Zhang, P. Li, X. Dai, Y. Xu, L. Liu, Evolution of soil properties following reclamation in coastal areas: a review, Geoderma 226 (2017) 130–139.
[44] J.P. Megonigal, W.H. Patrick Jr., S.P. Faulkner, Wetland identification in seasonally flooded forest soils: soil morphology and redox dynamics, Soil Sci. Soc. Am. 57 (1993) 140–149.
[45] E. Politi, S.K. Paterson, R. Scarrott, E. Tuohy, C. O'Mahony, W.C. Cámaro-García, Earth observation applications for coastal sustainability: potential and challenges for implementation, Anthropol. Rev. 2 (2019) 306–329.
[46] V. Klemas, Remote sensing of floods and flood-prone areas: an overview, J. Coast Res. 31 (2015) 1005–1013.
[47] W. Wu, C. Zhi, Y. Gao, C. Chen, Z. Chen, H. Su, W. Lu, B. Tian, Increasing fragmentation and squeezing of coastal wetlands: status, drivers, and sustainable protection from the perspective of remote sensing, Sci. Total Environ. 811 (2022) 152339.
[48] A. Zhang, G. Sun, P. Ma, X. Jia, J. Ren, H. Huang, X. Zhang, Coastal wetland mapping with Sentinel-2 MSI imagery based on gravitational optimized multilayer perceptron and morphological attribute profiles, Rem. Sens. 11 (2019) 952.
[49] E. Fluet-Chouinard, B. Lehner, L.M. Rebelo, F. Papa, S.K. Hamilton, Development of a global inundation map at high spatial resolution from topographic downscaling of coarse-scale remote sensing data, Remote Sens. Environ. 158 (2015) 348–361.
[50] R. Sadiq, Z. Akhtar, M. Imran, F. Ofli, Integrating remote sensing and social sensing for flood mapping, Remote Sens. Appl.: Soc. Environ. 25 (2022) 100697.
[51] S. Vitousek, D. Buscombe, K. Vos, P.L. Barnard, A.C. Ritchie, J.A. Warrick, The future of coastal monitoring through satellite remote sensing, Camb. Prism. Coast. Futures 1 (2023) e10.
[52] M. Benincasa, F. Falcini, C. Adduce, G. Sannino, R. Santoleri, Synergy of satellite remote sensing and numerical ocean modelling for coastal geomorphology diagnosis, Rem. Sens. 11 (2019) 2636.
[53] B. Deepika, K. Avinash, K. Jayappa, Shoreline change rate estimation and its forecast: remote sensing, geographical information system and statistics-based approach, Int. J. Environ. Sci. Technol. 11 (2014) 395–416.
[54] F. Pasquetti, M. Bini, A. Ciampalini, Accuracy of the TanDEM-X digital elevation model for coastal geomorphological studies in Patagonia (South Argentina), Rem. Sens. (11) (2019) 1767.
[55] C.A. Ruhl, D.H. Schoellhamer, R.P. Stumpf, C.L. Lindsay, Combined use of remote sensing and continuous monitoring to analyse the variability of suspended-sediment concentrations in San Francisco Bay, California, Estuar. Coast Shelf Sci. 53 (2001) 801–812.
[56] M. Umar, B.L. Rhoads, J.A. Greenberg, Use of multispectral satellite remote sensing to assess mixing of suspended sediment downstream of large river confluences, J. Hydrol. 556 (2018) 325–338.
[57] C. Wang, W. Li, S. Chen, D. Li, D. Wang, J. Liu, The spatial and temporal variation of total suspended solid concentration in Pearl River estuary during 1987–2015 based on remote sensing, Sci. Total Environ. 618 (2018) 1125–1138.
[58] B.M. Conroy, S.M. Hamylton, K. Kumbier, J.J. Kelleway, Assessing the structure of coastal forested wetland using field and remote sensing data, Estuar. Coast Shelf Sci. 271 (2022) 107861.
[59] M.L. Kirwan, K.B. Gedan, Sea-level driven land conversion and the formation of ghost forests, Nat. Clim. Change 9 (2019) 450–457.
[60] E.A. Ury, X. Yang, J.P. Wright, E.S. Bernhardt, Rapid deforestation of a coastal landscape driven by sea-level rise and extreme events, Ecol. Appl. 31 (2021) 02339.
[61] L.A. Freeman, D.R. Corbett, A.M. Fitzgerald, D.A. Lemley, A. Quigg, C.N. Steppe, Impacts of urbanization and development on estuarine ecosystems and water quality, Estuar. Coast 42 (2019) 1821–1838.
[62] Z. Zheng, Z. Wu, Y. Chen, Z. Yang, F. Marinello, Exploration of eco-environment and urbanization changes in coastal zones: a case study in China over the past 20 years, Ecol. Indicat. 119 (2020) 106–847.
[63] P.E. Zope, T.I. Eldho, V. Jothiprakash, Impacts of urbanization on flooding of a coastal urban catchment: a case study of Mumbai City, India, Nat. Hazards 75 (2015) 887–908.
[64] J.G. Barr, V. Engel, J.D. Fuentes, D.O. Fuller, H. Kwon, Modeling light use efficiency in a subtropical mangrove forest equipped with CO2 eddy covariance, Biogeosciences 10 (2013) 2145–2158.
[65] S.M. Decina, L.R. Hutyra, C.K. Gately, J.M. Getson, A.B. Reinmann, A.G.S. Gianotti, P.H. Templer, Soil respiration contributes substantially to urban carbon fluxes in the greater Boston area, Environ. Pollut. 212 (2016) 433–439.
[66] D. Liu, Y. Bai, X. He, B. Tao, D. Pan, C.T.A. Chen, L. Zhang, Y. Xu, C. Gong, Satellite estimation of particulate organic carbon flux from Changjiang River to the estuary, Remote Sens. Environ. 223 (2019) 307–319.
[67] P.C. Mohanty, S. Shetty, R.S. Mahendra, R.K. Nayak, L.K. Sharma, E.P. Rama Rao, Spatio-temporal changes of mangrove cover and its impact on bio-carbon flux along the West Bengal coast, Northeast coast of India, Eur. J. Remote Sens. 54 (2021) 525–537.
[68] J. Nogueira, H. Evangelista, L. Bouchaou, L. Moreira, A. Sifeddine, A. Elmouden, F. Msanda, S. Caquineau, F.J. Briceño-Zuluaga, M.V. Licínio, M. Mandeng-Yogo, Coastal wetland responses to a century of climate change in northern Sahara, Morocco, Limnol. Oceanogr. 67 (2022) 285–299.
[69] R.C. Zulueta, W.C. Oechel, J.G. Verfaillie, S.J. Hastings, B. Gioli, W.T. Lawrence, K.T. Paw U, Aircraft regional-scale flux measurements over complex landscapes of mangroves, desert, and marine ecosystems of Magdalena Bay, Mexico, J. Atmos. Ocean. Technol. 30 (2013) 1266–1294.
[70] A. Thieme, S. Yadav, P.C. Oddo, J.M. Fitz, S. McCartney, L. King, J. Keppler, G.W. McCarty, W.D. Hively, Using NASA Earth observations and Google Earth Engine to map winter cover crop conservation performance in the Chesapeake Bay watershed, Remote Sens. Environ. 248 (2020) 111943.
[71] R.M. Fanelli, J.D. Blomquist, R.M. Hirsch, Point sources and agricultural practices control spatial-temporal patterns of orthophosphate in tributaries to Chesapeake Bay, Sci. Total Environ. 652 (2019) 422–433.
[72] K.A. St Laurent, V.J. Coles, R.R. Hood, Climate extremes and variability surrounding Chesapeake Bay: past, present, and future, J. Am. Water Resour. Assoc. 58 (2021) 826–854.
[73] F. Cao, M. Tzortziou, C. Hu, A. Mannino, C.G. Fichot, R. Del Vecchio, R.G. Najjar, M. Novak, Remote sensing retrievals of colored dissolved organic matter and dissolved organic carbon dynamics in North American estuaries and their margins, Remote Sens. Environ. 205 (2018) 151–165.
[74] J.R. Holmquist, L. Windham-Myers, A conterminous USA-scale map of relative tidal marsh elevation, Estuar. Coast 45 (2022) 1596–1614.
[75] E. Stell, D. Warner, J. Jian, B. Bond-Lamberty, R. Vargas, Global Gridded 1-km Soil and Soil Heterotrophic Respiration Derived from SRDB v5, ORNL DAAC, Oak Ridge, Tennessee, USA, 2021.
[76] J. Jian, R. Vargas, K.J. Anderson-Teixeira, E. Stell, V. Herrmann, M. Horn, N. Kholod, J. Manzon, R. Marchesi, D. Paredes, B.P. Bond-Lamberty, A Global Database of Soil Respiration Data, Version 5.0, ORNL Distributed Active Archive Center, 2021.
[77] B. Bond-Lamberty, A. Thomson, A global database of soil respiration data, Biogeosciences 7 (2010) 1915–1926.
[78] M. Claverie, J. Ju, J.G. Masek, J.L. Dungan, E.F. Vermote, J.C. Roger, S.V. Skakun, C. Justice, The Harmonized Landsat and Sentinel-2 surface reflectance data set, Remote Sens. Environ. 219 (2018) 145–161.
[79] G. Camps-Valls, M. Campos-Taberner, Á. Moreno-Martínez, S. Walther, G. Duveiller, A. Cescatti, M.D. Mahecha, J. Muñoz-Marí, F.J. García-Haro, L. Guanter, M. Jung, A unified vegetation index for quantifying the terrestrial biosphere, Sci. Adi. 7 (2021) eabc7447.
[80] N. Huang, L. Wang, X.P. Song, T.A. Black, R.S. Jassal, R.B. Myneni, C. Wu, L. Wang, W. Song, D. Ji, S. Yu, Spatial and temporal variations in global soil respiration and their relationships with climate and land cover, Sci. Adv. 6 (2020) eabb8508.
[81] J.W. Raich, W.H. Schlesinger, The global carbon dioxide flux in soil respiration and its relationship to vegetation and climate, Tellus B 44 (1992) 81–99.
[82] L.E. Rustad, T.G. Huntington, R.D. Boone, Controls on soil respiration: implications for climate change, Biogeochemistry 48 (2000) 1–6.
[83] M.M. Thornton, R. Shrestha, Y. Wei, P.E. Thornton, S.-C. Kao, B.E. Wilson, Daymet: Annual Climate Summaries on a 1-km Grid for North America, Version 4 R1, ORNL DAAC, Oak Ridge, Tennessee, USA, 2022.
[84] J. Dewitz, U.S. Geological Survey, National land cover database (NLCD) 2019 products (ver. 2.0, June 2021), U.S. Geological Survey data release (2021).
[85] C.E. Shannon, A mathematical theory of communication, Bell Syst. Tech. J. 27 (1948) 379–423.
[86] L.J. Sugarbaker, E.W. Constance, H.K. Heidemann, J.A. Jason, Vicki Lukas, D.L. Saghy, J.M. Stoker, The 3D Elevation Program initiative: a call for action, U.S. Geological Survey (2014).

[87] I.D. Moore, R.B. Grayson, A.R. Ladson, Digital terrain modeling: a review of hydrological, geomorphological, and biological applications, Hydrol. Process. 5 (1991) 3–30.
[88] A. Ramcharan, T. Hengl, T. Nauman, C. Brungard, S. Waltman, S. Wills, J. Thompson, Soil property and class maps of the conterminous United States at 100-meter spatial resolution, Soil Sci. Soc. Am. J. 82 (2018) 186–201.
[89] F. Murtagh, P. Contreras, Algorithms for hierarchical clustering: an overview, Wiley Interdisc. Rev. Data Min. Knowl. Discovery 2 (2012) 86–97.
[90] A. Ferrer, K.D. Heath, T. Canam, H.D. Flores, J.W. Dalling, Contribution of fungal and invertebrate communities to wood decay in tropical terrestrial and aquatic habitats, Ecology 101 (2020) e03097.
[91] E. Barshan, A. Ghodsi, Z. Azimifar, M.Z. Jahromi, Supervised principal component analysis: Visualization, classification and regression on subspaces and submanifolds, Pattern Recogn. 44 (2011) 1357–1371.
[92] S. Zhou, Z. Xu, F. Liu, Method for determining the optimal number of clusters based on agglomerative hierarchical clustering, IEEE Transact. Neural Networks Learn. Syst. 28 (2016) 3007–3017.
[93] A.G.S.J. Baccini, S.J. Goetz, W.S. Walker, N.T. Laporte, M. Sun, D. Sulla-Menashe, J. Hackler, P.S.A. Beck, R. Dubayah, M.A. Friedl, S. Samanta, Estimated carbon dioxide emissions from tropical deforestation improved by carbon-density maps, Nat. Clim. Change (2) (2012) 182–185.
[94] M. Jung, M. Reichstein, C.R. Schwalm, C. Huntingford, S. Sitch, A. Ahlström, A. Arneth, G. Camps-Valls, P. Ciais, P. Friedlingstein, F. Gans, Compensatory water effects link yearly global land CO2 sink changes to temperature, Nature 541 (2017) 516–520.
[95] L. Zhong, L. Hu, H. Zhou, Deep learning based multi-temporal crop classification, Remote Sens. Environ. 221 (2019) 430–443.
[96] S.M. Lundberg, S.I. Lee, A unified approach to interpreting model predictions, Adv. Neural Inf. Process. Syst. (2017) 30.
[97] S.M. Lundberg, G. Erion, H. Chen, A. DeGrave, J.M. Prutkin, B. Nair, R. Katz, J. Himmelfarb, N. Bansal, S.I. Lee, From local explanations to global understanding with explainable AI for trees, Nat. Mach. Intell. 2 (2020) 56–67.
[98] B.J. Biggs, V.I. Nikora, T.H. Snelder, Linking scales of flow variability to lotic ecosystem structure and function, River Res. Appl. 21 (2005) 283–298.
[99] J.E. Hewitt, S.F. Thrush, P.D. Dayton, Habitat variation, species diversity and ecological functioning in a marine system, J. Exp. Mar. Biol. Ecol. 366 (2008) 116–122.
[100] A.L. Hinson, R.A. Feagin, M. Eriksson, R.G. Najjar, M. Herrmann, T.S. Bianchi, M. Kemp, J.A. Hutchings, S. Crooks, T. Boutton, The spatial distribution of soil organic carbon in tidal wetland soils of the continental United States, Global Change Biol. 23 (2017) 5468–5480.
[101] M.J. Osland, C.A. Gabler, J.B. Grace, R.H. Day, M.L. McCoy, J.L. McLeod, A.S. From, N.M. Enwright, L.C. Feher, C.L. Stagg, S.B. Hartley, Climate and plant controls on soil organic matter in coastal wetlands, Global Change Biol. 24 (2018) 5361–5379.
[102] A.V.I. Shmida, M.V. Wilson, Biological determinants of species diversity, J. Biogeogr. (1985) 1–20.
[103] B. Naseri, Charcoal rot of bean in diverse cropping systems and soil environments, J. Plant Dis. Prot. 121 (2014) 20–25.
[104] W.A.G.D.A. Nunes, J.F.S. Menezes, V.D.M. Benites, S.A.D. Lima Junior, A.D.S. Oliveira, Use of organic compost produced from slaughterhouse waste as fertilizer in soybean and corn crops, Sci. Agric. 72 (2015) 343–350.
[105] S.A. Materechera, A.M. Alston, J.M. Kirby, A.R. Dexter, Influence of root diameter on the penetration of seminal roots into compacted subsoil, Plant Soil 144 (1992) 297–303.
[106] S.A. Materechera, A.R. Dexter, A.M. Alston, Penetration of very strong soils by seedling roots of different plant species, Plant Soil 135 (1991) 31–34.
[107] J. Schwaab, R. Meier, G. Mussetti, S. Seneviratne, C. Bürgi, E.L. Davin, The role of urban trees in reducing land surface temperatures in European cities, Nat. Commun. 12 (2021) 6763.
[108] J. Iqbal, R. Hu, M. Feng, S. Lin, S. Malghani, I.M. Ali, Microbial biomass, and dissolved organic carbon and nitrogen strongly affect soil respiration in different land uses: a case study at Three Gorges Reservoir Area, South China, Agric. Ecosyst. Environ. 137 (2010) 294–307.
[109] L.D. Brin, A.E. Giblin, J.J. Rich, Effects of experimental warming and carbon addition on nitrate reduction and respiration in coastal sediments, Biogeochemistry 125 (2015) 81–95.
[110] L.G. Chambers, S.E. Davis, T. Troxler, J.N. Boyer, A. Downey-Wall, L.J. Scinto, Biogeochemical effects of simulated sea level rise on carbon loss in an Everglades mangrove peat soil, Hydrobiologia 726 (2014) 195–211.
[111] D.M. Martin, A.D. Jacobs, C. McLean, M.R. Canick, K. Boomer, Using structured decision making to evaluate wetland restoration opportunities in the Chesapeake Bay Watershed, Environ. Manag. 70 (2022) 950–964.
[112] D. Scavia, I. Bertani, J.M. Testa, A.J. Bever, J.D. Blomquist, M.A. Friedrichs, L.C. Linker, B.D. Michael, R.R. Murphy, G.W. Shenk, Advancing estuarine ecological forecasts: seasonal hypoxia in Chesapeake Bay, Ecol. Appl. 31 (2021) e02384.
[113] D.C. Walters, J.A. Carr, A. Hockaday, J.A. Jones, E. McFarland, K.E. Kovalenko, M.L. Kirwan, D.R. Cahoon, G.R. Guntenspergen, Experimental tree mortality does not induce marsh transgression in a Chesapeake Bay low-lying coastal forest, Front. Mar. Sci. 8 (2021) 782, 643.
[114] E.A. Davidson, I.A. Janssens, Temperature sensitivity of soil carbon decomposition and feedbacks to climate change, Nature 440 (2006) 165–173.
[115] A.M. Oliverio, M.A. Bradford, N. Fierer, Identifying the microbial taxa that consistently respond to soil warming across time and space, Global Change Biol. 23 (2017) 2117–2129.
[116] M.A. Bradford, Thermal adaptation of decomposer communities in warming soils, Front. Microbiol. 4 (2013) 333.
[117] C.J. Williams, Y. Yamashita, H.F. Wilson, R. Jaffé, M.A. Xenopoulos, Unraveling the role of land use and microbial activity in shaping dissolved organic matter characteristics in stream ecosystems, Limnol. Oceanogr. 55 (2010) 1159–1171.
[118] R.P. Wolkowski, Relationship between wheel-traffic-induced soil compaction, nutrient availability, and crop growth: a review, J. Prod. Agric. 3 (1990) 460–469.
[119] H.J. Wu, X. Lee, Short-term effects of rain on soil respiration in two New England forests, Plant Soil 338 (2011) 329–342.
[120] R.G. Najjar, C.R. Pyke, M.B. Adams, D. Breitburg, C. Hershner, M. Kemp, R. Howarth, M. Mulholland, M. Paolisso, D. Secor, K. Sellner, Potential climate-change impacts on the Chesapeake Bay, Estuar. Coast Shelf Sci. 86 (2010) 1–20.
[121] E.D. Schulze, H.A. Mooney, O.E. Sala, E. Jobbagy, N. Buchmann, G. Bauer, J. Canadell, R.B. Jackson, J. Loreti, M. Oesterheld, J.R. Ehleringer, Rooting depth, water availability, and vegetation cover along an aridity gradient in Patagonia, Oecologia 108 (1996) 503–511.
[122] S.D. Wullschleger, F.C. Meinzer, R.A. Vertessy, A review of whole-plant water use studies in tree, Plant Physiol. 18 (1998) 499–512.
[123] A.M. Hopple, K.O. Doro, V.L. Bailey, B. Bond-Lamberty, N. McDowell, K.A. Morris, A. Myers-Pigg, S.C. Pennington, P. Regier, R. Rich, A. Sengupta, Attaining freshwater and estuarine-water soil saturation in an ecosystem-scale coastal flooding experiment, Environ. Monit. Assess. 195 (2023) 425.
[124] S.C. Pennington, N.G. McDowell, J.P. Megonigal, J.C. Stegen, B. Bond-Lamberty, Localized basal area affects soil respiration temperature sensitivity in a coastal deciduous forest, Biogeosciences 17 (3) (2020) 771–780.
[125] D.A. Riveros-Iregui, B.L. McGlynn, R.E. Emanuel, H.E. Epstein, Complex terrain leads to bidirectional responses of soil respiration to inter-annual water availability, Global Change Biol. 18 (2012) 749–756.
[126] M.B. Wagena, A.S. Collick, A.C. Ross, R.G. Najjar, B. Rau, A.R. Sommerlot, D.R. Fuka, P.J. Kleinman, Z.M. Easton, Impact of climate change and climate anomalies on hydrologic and biogeochemical processes in an agricultural catchment of the Chesapeake Bay watershed, USA, Sci. Total Environ. 637 (2018) 1443–1454.
[127] G.B. Noe, M.J. Cashman, K. Skalak, A. Gellis, K.G. Hopkins, D. Moyer, J. Webber, A. Benthem, K. Maloney, J. Brakebill, A. Sekellick, Sediment dynamics and implications for management: state of the science from long-term research in the Chesapeake Bay watershed, USA, Wiley Interdisciplinary Reviews: Water 7 (4) (2020) e1454.
[128] Z.F. Lund, Available water-holding capacity of alluvial soils in Louisiana, Soil Sci. Soc. Am. J. 23 (1959) 1–3.
[129] M.B. McBride, Environmental Chemistry of Soils, Oxford Univ. Press, New York, 1994.
[130] Y. Rong, L. Ma, D.A. Johnson, F. Yuan, Soil respiration patterns for four major land-use types of the agro-pastoral region of northern China, Agric. Ecosyst. Environ. 213 (2015) 142–150.
[131] G. Gelybó, Z. Barcza, M. Dencsö, I. Potyó, I. Kása, Á. Horel, K. Pokovai, M. Birkás, A. Kern, R. Hollós, E. Tóth, Effect of tillage and crop type on soil respiration in a long-term field experiment on chernozem soil under temperate climate, Soil Tillage Res. 216 (2022) 105239.

[132] E. Pareja-Sánchez, C. Cantero-Martínez, J. Álvaro-Fuentes, D. Plaza-Bonilla, Tillage and nitrogen fertilization in irrigated maize: key practices to reduce soil CO2 and CH4 emissions, Soil Tillage Res. 191 (2019) 29–36.
[133] G. Gelybó, Z. Barcza, M. Dencső, I. Potyó, I. Kása, Á. Horel, K. Pokovai, M. Birkás, A. Kern, R. Hollós, E. Tóth, Effect of tillage and crop type on soil respiration in a long-term field experiment on chernozem soil under temperate climate, Soil Tillage Res. 216 (2022) 105239.
[134] Y. Luo, X. Zhou, Soil Respiration and the Environment, Academic Press, San Diego, California, USA, 2010.
[135] P. Vanhala, Seasonal variation in the soil respiration rate in coniferous forest soils, Soil Biol. Biochem. 34 (2002) 1375–1379.
[136] E.J. Sayer, Using experimental manipulation to assess the roles of leaf litter in the functioning of forest ecosystems, Biol. Rev. 81 (2006) 1–31.
[137] W.J. Wang, R.C. Dalal, P.W. Moody, C.J. Smith, Relationships of soil respiration to microbial biomass, substrate availability and clay content, Soil Biol. Biochem. 35 (2003) 273–284.
[138] E.M. Morrissey, J.L. Gillespie, J.C. Morina, R.B. Franklin, Salinity affects microbial activity and soil organic matter content in tidal wetlands, Global Change Biol. 20 (2014) 1351–1362.
[139] P. Roychand, Addition of clay to sand – effect of clay concentration, water content and bulk density on soil respiration, Agrochimica Pisa 61 (2017) 1–12.
[140] M.S. Sax, N. Bassuk, H. van Es, D. Rakow, Long-term remediation of compacted urban soils by physical fracturing and incorporation of compost, Urban For. Urban Green. 24 (2017) 149–156.
[141] N.D. Bettez, P.M. Groffman, Denitrification potential in stormwater control structures and natural riparian zones in an urban landscape, Environ. Sci. amp; Technol. 46 (2012) 10909–10917.
[142] G. Miao, A. Noormets, J.C. Domec, C.C. Trettin, S.G. McNulty, G. Sun, J.S. King, The effect of water table fluctuation on soil respiration in a lower coastal plain forested wetland in the southeastern US, J. Geophys. Res. Biogeosci. 118 (2013) 1748–1762.
[143] G. Chen, J. Bai, J. Wang, Z. Liu, B. Cui, Responses of soil respiration to simulated groundwater table and salinity fluctuations in tidal freshwater, brackish and salt marshes, J. Hydrol. 612 (2022) 128215.
[144] L. Tan, Z. Ge, Y. Ji, D.Y. Lai, S. Temmerman, S. Li, X. Li, J. Tang, Land use and land cover changes in coastal and inland wetlands cause soil carbon and nitrogen loss, Global Ecol. Biogeogr. 31 (2022) 2541–2563.